Chemical Geology 584 (2021) 120538

Contents lists available at ScienceDirect

Chemical Geology

journal homepage: www.elsevier.com/locate/chemgeo

A sequential extraction procedure for particulate manganese and its application to coastal marine sediments

W.K. Lenstra *, R. Klomp, F. Molema, T. Behrends, C.P. Slomp

Department of Earth Sciences – Geochemistry, Utrecht University, PO Box 80021, 3508 TA Utrecht, The Netherlands

ARTICLE INFO

Editor: Michael E. Boettcher

Keywords:
Manganese
Sequential extraction
Sediment
Manganese standards

ABSTRACT

An existing sequential extraction scheme for particulate iron (Fe) is evaluated for manganese (Mn) using a range of Mn standards. The scheme consists of 5 steps and quantifies 5 operationally defined Mn pools (1) poorly ordered Mn oxides and Mn phosphates (ascorbic acid extractable); (2) Mn carbonates and Mn sulfides (1 M HCl extractable), (3 and 4) crystalline Mn oxides (citrate buffered dithionite and ammonium oxalate extractable, respectively) and (5) Mn associated with pyrite (concentrated HNO_3 extractable). Application of the extraction scheme to coastal sediments from six locations (Black Sea, Baltic Sea, Bothnian Sea, Gulf of Mexico and Chesapeake Bay) highlights the dependency of sediment Mn partitioning on bottom water redox conditions. In sediments deposited in anoxic and sulfidic (euxinic) bottom waters, Mn is mostly present in Mn carbonates, pyrite and in non-reactive Mn forms, in approximately equal amounts. We find that in sediments deposited in periodically euxinic and hypoxic (oxygen $<63\ \mu mol\ L^{-1}$) waters, Mn carbonates dominate over the two other fractions, and small amounts of Mn oxides are observed. In sediments deposited in oxygenated bottom waters, Mn oxides, Mn-rich vivianite-type minerals and Mn carbonates dominate and no pyrite-bound Mn is observed. A large advantage of the extraction scheme is that it quantifies sediment forms of Mn and Fe simultaneously. Given the role of Mn as a bottom water redox proxy, the separation of poorly ordered Mn oxides, carbonates and pyrite is of specific relevance.

1. Introduction

Manganese (Mn) is a key micro-nutrient in marine surface waters (Raven, 1990; Moore et al., 2013). The cycling of Mn in the marine environment interacts with that of iron (Fe), carbon, phosphorus, nitrogen, sulfur and various trace metals (Burdige, 1993; Canfield et al., 1993; Luther et al., 1997; Beal et al., 2009). For example, Mn oxides can act as an electron acceptor in the oxidation of organic matter and as a carrier for phosphorus, cobalt and nickel (Goldberg, 1954; Koschinsky and Hein, 2003; Jilbert and Slomp, 2013). In ancient sediments, Mn contents are frequently used as a proxy of bottom water oxygen concentrations (i.e. Calvert and Pedersen (1993), Johnson et al. (2016), Ostrander et al. (2019)). With the present-day expansion of low oxygen areas in the open and coastal ocean (Breitburg et al., 2018), detailed insight into the forms of Mn in sediments and the water column and their response to environmental changes is becoming increasingly important.

In oxic waters and surface sediments, particulate Mn is mainly present in the form of Mn oxides (Fig. 1; Calvert and Pedersen (1993), Burdige (1993)). These Mn oxides can consist of minerals within the group of tecto- and phyllomanganates such as birnessite and pyrolusite or crystalline forms such as manganite and bixbyite (Hem and Lind, 1983; Anschutz et al., 2005). Upon burial or downward mixing by macrofauna, Mn oxides can be reductively dissolved during the degradation of organic matter or through reactions with sulfide (H_2S), dissolved Fe(II) or CH_4 (Postma, 1985; Burdige, 1993; Beal et al., 2009). This leads to release of dissolved Mn to the porewater, either as Mn(II) or Mn(III) (Madison et al., 2013). Upward diffusing dissolved Mn(II) and Mn(III) can be re-oxidized in the oxic surface sediment and again form Mn oxides (Sundby and Silverberg, 1985; Learman et al., 2011). In anoxic sediments, where dissolved Mn(II) and carbonate (CO_3^{2-}) concentrations in porewaters are high, red$MnCO_3$ or mixed Mn-Mg-Ca carbonate phases, such as rhodochrosite or pseudokutnahorite, may form (Middelburg et al., 1987; Mucci, 1988; Neumann et al., 2002). In coastal sediments with a low salinity, vivianite-type minerals rich in Mn ($(Fe, Mn)_3(PO_4)_2 \cdot 4H_2O$) can contribute to burial of Mn (Nakano, 1992; Egger et al., 2015; Lenstra et al., 2018). In sulfidic sediments, part of the dissolved Mn can be incorporated in pyrite or in authigenic Mn sulfide

* Corresponding author.
E-mail address: w.k.lenstra@uu.nl (W.K. Lenstra).

https://doi.org/10.1016/j.chemgeo.2021.120538
Received 18 June 2021; Received in revised form 17 September 2021; Accepted 20 September 2021
Available online 24 September 2021

minerals, such as alabandite and rambergite, (Suess, 1979; Lepland and Stevens, 1998; Huerta-Diaz and Morse, 1992; Lenstra et al., 2020). A small fraction of non-reactive Mn can be present in clays, such as smectites and primary Fe-Mg silicates.

Changes in particulate Mn forms with depth and time in sediments and the water column are frequently inferred from trends in total Mn contents (i.e. Lyons and Severmann (2006), Dellwig et al. (2007), Sulu-Gambari et al. (2017)). For example, when oxic marine bottom waters transition into anoxia, surface sediments typically become depleted of Mn (Calvert and Pedersen, 1993; Brumsack, 2006). This is usually attributed to reductive dissolution of Mn oxides and escape of the dissolved Mn to the water column (Sulu-Gambari et al., 2017; Hermans et al., 2021). This dissolved Mn may then precipitate again as Mn oxide in the water column upon contact with oxygen in the redoxcline and the Mn oxide may then settle on the seafloor. Analyses of the chemical and mineral composition of particulate Mn from marine environments with XRD, synchotron-based X-ray spectroscopy and SEM-EDS have confirmed such redox driven cycles. (Lenz et al., 2014; Lenstra et al., 2020; Lee et al., 2021). While these latter methods allow the identification and, in suspended matter, quantification of Mn minerals, these techniques are rather time-intensive (e.g. Lam et al. (2015)). Hence, they can typically only be carried out for a subset of samples and need to be complemented with bulk geochemical analyses by wet chemical techniques. Various single step and sequential procedures for the extraction of particulate Mn have been proposed (Tessier et al., 1979; Hyacinthe et al., 2001; Hyacinthe and Van Cappellen, 2004; Anschutz et al., 2005; Mouret et al., 2009). However, to date, these methods have not been applied in a sequential scheme, calibrated with standards for key Mn minerals.

In this study, we present a 5-step sequential extraction procedure for Mn, which we apply to a total of sixteen standards that include various types of Mn oxides, Mn phosphates, Mn carbonate, Mn sulfide and clays. This procedure combines steps from three sequential extraction schemes used for the partitioning of solid phase Fe (Poulton and Canfield, 2005; Claff et al., 2010; Raiswell et al., 2010) as presented by Lenstra et al. (2019) in a study of Black Sea sediments and suspended matter. We demonstrate that the method is particularly successful in separating poorly ordered Mn oxides, Mn carbonates and Mn in pyrite. By applying the method to a range of coastal sediments, we further demonstrate its suitability in distinguishing particulate Mn phases.

2. Material and methods

2.1. Mn extraction scheme

The 5-step sequential extraction procedure applied in this study (Table 1) employs (1) ascorbic acid (pH 7.5) to extract poorly ordered Mn oxides such as birnessite and pyrolusite (Raiswell et al., 2010; Hyacinthe and Van Cappellen, 2004); (2) 1 M HCl to dissolve metal carbonates (Claff et al., 2010); (3) citrate buffered dithionite and (4) ammonium oxalate to extract crystalline metal oxides (Poulton and Canfield, 2005) and (5) concentrated HNO_3 to extract Mn bound in pyrite (Huerta-Diaz and Morse, 1992; Claff et al., 2010). All solutions

Table 1
Sequential extraction procedure based on Raiswell et al. (2010), Poulton and Canfield (2005) and Claff et al. (2010) as presented in Lenstra et al. (2019). All extraction steps were performed at room temperature.

Step	Extractant	Time (h)	Terminology	Reference
1	0.17 M sodium citrate, 0.6 M sodium bicarbonate and 0.057 M ascorbic acid (pH 7.5)	24	Mn Asc.	Raiswell et al. (2010)
2	1 M HCl	4	Mn HCl	Huerta-Diaz and Morse (1990)
3	50 g L^{-1} sodium dithionite solution buffered to pH 4.8 with 0.35 M acetic acid/ 0.2 M sodium citrate	4	Mn CDB	Poulton and Canfield (2005)
4	0.2 M ammonium oxalate/ 0.17 M oxalic acid (pH 3.2)	6	Mn Oxalate	Poulton and Canfield (2005)
5	65% HNO_3	2	Mn HNO_3	Lord (1982), Claff et al. (2010)

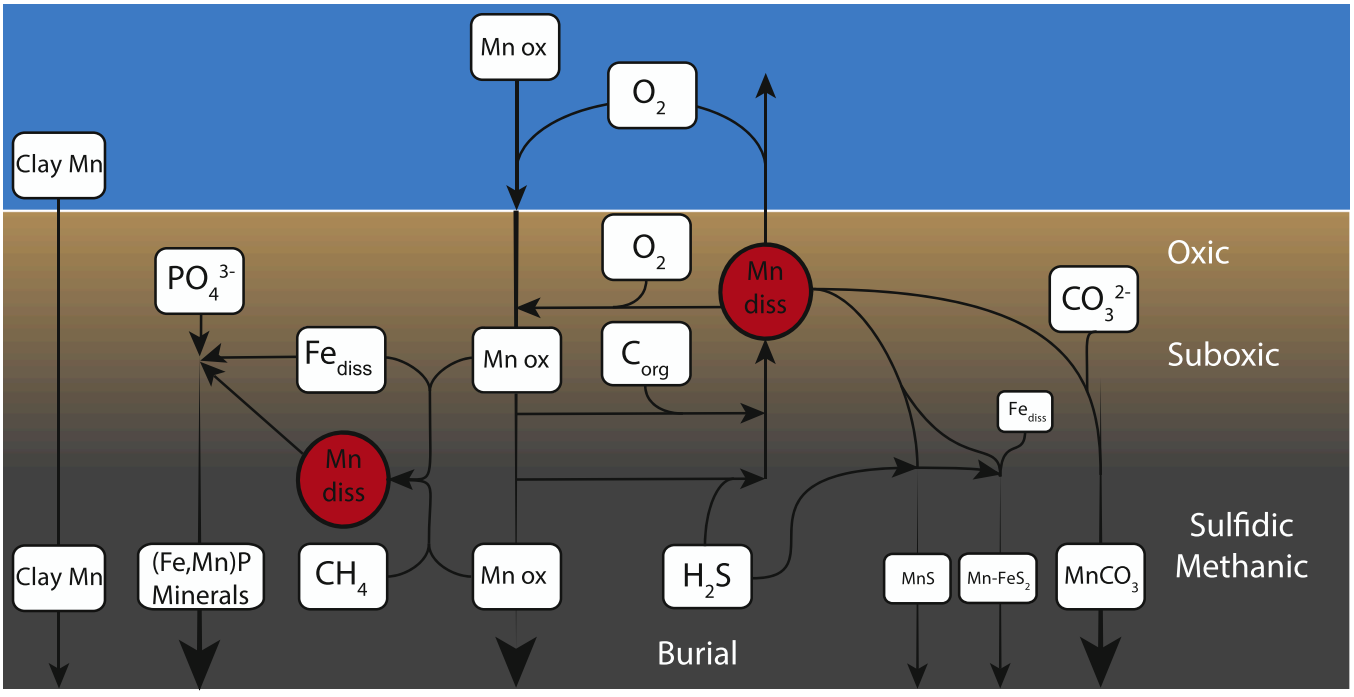

Fig. 1. Schematic overview of Mn dynamics in coastal sediments. Mn ox: Mn oxides, Clay Mn: Mn associated with clays, Mn_{diss}: dissolved Mn, C_{org}: organic carbon, Fe_{diss}: dissolved Fe, Mn-FeS_2: Mn associated with pyrite, MnS: Mn sulfides, $MnCO_3$: Mn carbonates.

were deoxygenated before addition to the samples, except for the concentrated HNO_3 solution. All reagents used during the sequential extraction procedure were analytical grade and the solutions were prepared using deionised (Milli-Q) water.

Aliquots of ca. 20 mg of each Mn standard (in triplicate) and 100 mg of each sediment sample were subjected to 10 ml of extractant in each step. During the extraction the samples were shaken on a shaker table. After extraction, all solutions were centrifuged and subsequently passed through a 0.45 μm nylon filter except for the concentrated HNO_3 solution. Concentrations of Mn were analyzed by Inductively Coupled Plasma Optical Emission Spectroscopy (ICP-OES; Spectro Arcos).

To gain insight in the dissolution kinetics of Mn oxides and Mn phosphate during the 24 h extraction with ascorbic acid (Step 1; Table 1), experiments where performed using birnissite, manganite and Mn bearing vivianite (Mn/Fe ratio: 0.1) standard. All Mn experiments were carried out in triplicate on ca. 20 mg of the Mn standards using 10 ml of extractant. During this extraction 5 samples were taken with time at 0, 1.1, 2.55, 4.45, 6.35 and 24 h after the start.

2.2. Mn standards

The sixteen Mn standards consist of six different types of Mn oxides, capturing various crystallinities and redox states, a range of six vivianite-type minerals ($(Fe, Mn)_3(PO_4)_2 \cdot 4H_2O$) with varying ratios of Fe and Mn, a Mn carbonate (rhodochrosite), a Mn sulfide (alabanite) and two clay samples (two types of smectite; Table 2). One of the amourphous Mn oxide standards was obtained from a Mn nodule.

The vivianite-type minerals were synthesized by mixing a 0.2 M Mohr salt solution ($(NH_4)_2Fe(SO_4)_2\ 6H_2O$) with a solution of 0.16 M ammonium acetate and 0.47 M disodium phosphate in an argon filled glovebox (1:1 volume ratio) following the procedure described by Rouzies and Millet (1993). To synthesize vivianite-type minerals with varying Mn concentrations, we added 0.6 M $MnCl_2$ solution in various ratios to the solutions following Dijkstra et al. (2018a), and always kept the P:(Fe+Mn) ratio at 1:1. All chemical solutions were deoxygenated before mixing and prepared in sulfate-free artificial seawater with a salinity of 14, as in Dijkstra et al. (2018a). Artificial seawater was prepared according to Millero (1974) after Kester et al. (1967). After combining the Fe, Mn and phosphate containing solutions, these were shaken for 48 h under an argon atmosphere. Subsequently, the supernatant was removed by centrifuging and the minerals were washed twice with deoxygenated water and dried under an argon atmosphere for 7 days.

To determine the total elemental concentrations of the Mn standards, all standards were ground in an agate mortar and ca. 10 mg was digested in 2.5 ml mixed acid (HNO_3:$HClO_4$; 2:3) and 2.5 ml 40% HF at 90 °C. After fuming off the acids, the residue was redissolved in 2.5 ml concentrated H_2O_2 and 2.5 ml concentrated HCl. After fuming off the H_2O_2 and HCl, the residue was redissolved in 1 M HNO_3. The solutions were subsequently analyzed for total Al, Ca, Fe, Mn, P, S and Ti by ICP-OES. The average analytical uncertainty based on duplicates was 6% for Mn.

The mineralogy of all Mn standards was determined by X-ray diffraction (XRD) using a Bruker D2 diffractometer with Cobalt Kα radiation over a 5–85 2σ range with a step size of 0.026°. The characterization of the Mn standards using XRD is described in Supplementary Information (Fig. A.1).

2.3. Sediment collection and analyses

The sequential extraction scheme was applied to coastal sediments from six sites, which were selected to capture a range of bottom water redox conditions (Table 3). The sites are located in the euxinic Northern Gotland basin in the Baltic Sea (LL19), the seasonally hypoxic Gulf of Finland (GoF5), the oxic deep basin of the Bothnian Sea (US5B), the hypoxic shelf edge near the chemocline in the northwestern Black Sea (Black Sea 6), the seasonally hypoxic Louisiana shelf in the Gulf of Mexico (GoM1) and an oxic estuary in Chesapeake Bay (ET5.1).

Table 2
Source and total elemental concentrations of the manganese standards included in this study, bdl is below detection limit. The Mn minerals were characterized with XRD (Fig. A.1). The low amount of sample used (i.e. 10 mg) for the determination of the total element composition might lead to some uncertainties in these numbers.

Standard XRD characterization[a]	Source	Al μmol g^{-1}	Ca μmol g^{-1}	Fe μmol g^{-1}	Mn μmol g^{-1}	P μmol g^{-1}	S μmol g^{-1}	Ti μmol g^{-1}
Mn(IV) oxide								
Mn nodule	In house collection	1349	303	2668	2238	71	147	135
Pyrolusite	Alfa Aesar	402	590	29	6994	72	bdl	bdl
Mn(IV/III) oxide								
Birnessite	LGIT[b]	366	32	13	10,491	bdl	342	bdl
Mn(III) oxide								
Manganite	Ward	351	53	360	2125	bdl	bdl	bdl
Bixbyite	Alfa Aesar	352	35	13	12,231	bdl	bdl	bdl
Mn(II/III) oxide								
Hausmannite	Alfa Aesar	368	49	42	5921	bdl	bdl	bdl
Mn(II) phosphate								
Hureaulite	Alfa Aesar	115	307	9	5970	5768	382	bdl
Switzerite	Synthesis	401	67	27	5663	4403	bdl	bdl
Mn/Fe (6)	Synthesis	341	44	892	5369	3993	32	bdl
Mn/Fe (2)	Synthesis	68	117	2322	4558	4397	244	bdl
Mn/Fe (0.5)	Synthesis	353	21	3834	1976	3808	191	bdl
Mn/Fe (0.1)	Synthesis	403	20	5179	560	3603	427	bdl
Mn carbonate								
Rhodochrosite	Baker	401	41	25	9154	bdl	bdl	bdl
Mn(II) sulfide								
Alabanite	Alfa Aesar	254	41	29	10,577	bdl	8235	bdl
Clay								
Smectite-1	Clay mineral society	3706	108	773	5	27	218	104
Smectite-2	Clay mineral society	2581	332	2287	3	38	490	84

[a] XRD characterization: main mineral observed by XRD, complete overview is given in the appendix and Fig. A.1
[b] Laboratoire de Géophysique Interne et Tectonophysique.

Table 3
Location and site characteristics of the six sites included in this study, BW is bottom water.

Basin	Label	Latitude N	Longitude	Depth mbss	Organic carbon* wt %	BW oxygen μmol L^{-1}	BW salinity	Year of sampling	Reference
Baltic Sea	LL19	58°53.24′	20°19.5′ E	173	9.6	0 (H_2S: 6.3)	11.7	2016	[a]
Baltic Sea	GoF5	59°57.10′	25°11.02′ E	65	10.4	11	9.4	2016	[b]
Black Sea	Black Sea 6	43°45.9′	30°05.1′ E	114	0.9	27	20	2015	[c]
Gulf of Mexico**	GoM1	28°48.55′	91°20.12′ W	16	0.8	56	35.6	2018	[d]
Bothnian Sea	US5B	62°35.17′	19°58.13′ E	214	3.2	180	6	2013	[e]
Chesapeake Bay	ET5.1	38°48.36′	75°54.66′ W	4	6.2	339	5.2	2017	[f]

[a] Lenstra et al. (2021).
[b] Hermans et al. (2021).
[c] Lenstra et al. (2020).
[d] Lenstra et al., in prep.
[e] Egger et al. (2015).
[f] Kubeneck et al. (2021).
* Organic carbon contents in the surface sediment (0–0.5 cm) for all stations except for US5B (0–1 cm).
** Methods as in Lenstra et al. (2019).

Sediment depth profiles of organic carbon, total Mn, and pyrite, and porewater profiles of dissolved Mn and H_2S determined for these sites were all previously published except for site GoM1 in the Gulf of Mexico (Table 3). We briefly summarize the methods here. At each site, a sediment core was collected and sliced under a nitrogen atmosphere. Porewater was extracted via centrifugation and sediments were subsequently freeze-dried and ground in an agate mortar under an argon atmosphere. Total Mn in the sediment was determined through dissolution with HF and HNO_3 and analyzed with an ICP-OES as described in Section 2.2. Organic carbon contents were determined on a NCS analyzer after decalcification. Pyrite was determined as chromium reducible sulfur. For further details on the procedures for site GoM1, we refer to Lenstra et al. (2019).

The bottom water salinity at the sites, as determined with a CTD system at the time of sampling, ranged from 5.2 at ET5.1 to 35.6 at GoM1 (Table 3). Organic carbon contents in the surface sediment ranged from 0.8 wt% at GoM1 to 10.4 wt% at GoF5 (Table 3). Sediments at all sites contained pyrite (Fig. A.2), with highest concentrations at the euxinic (LL19) and seasonally hypoxic site in the Baltic Sea (GoF5). Dissolved porewater Fe was lowest at the euxinic sites and highest at the oxic sites (Fig. A.2).

3. Results and discussion

3.1. Sequential extraction of Mn standards

The application of the 5-step sequential extraction procedure (Table 1) to the sixteen Mn standards (Table 2) revealed distinct differences in the solubility of the various Mn forms (Fig. 2; Table A.1). The ascorbic acid solution (Step 1), efficiently extracted the tecto- and phyllomanganates birnessite (99%) and pyrolusite (87%) and the amorphous Mn oxides in the nodule (88%), but only partially dissolved the crystalline Mn oxides manganite (49%), bixbyite (48%) and hausmannite (40%). This indicates that not all Mn oxides are necessarily dissolved during a 24 h extraction with ascorbic acid. This contrasts with the observations of Hyacinthe and Van Cappellen (2004) who reported efficient extraction of birnissite, bixyite, hausmannite and pyrolusite using this procedure. The difference might be related to

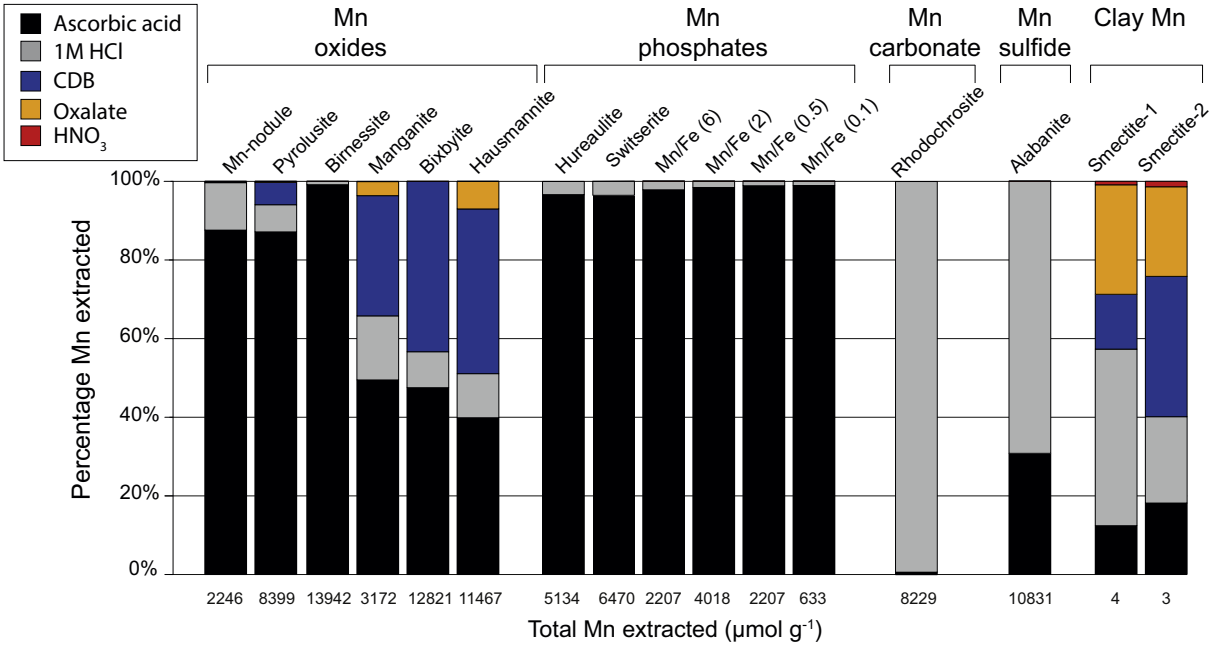

Fig. 2. Percentages of Mn extracted from sixteen standards (Table 2) during the 5-step sequential extraction procedure (Table 1). Total extracted Mn during the procedure for the different standards is given at the bottom of each bar in μmol g^{-1}. Percentages and values are means of triplicate analyses. Amounts of Mn extracted, including standard deviations for all extraction steps are presented in Table A.1.

differences in the composition of the Mn standards and/or differences in ageing (Eitel et al., 2018), which might especially affect the extraction of Mn minerals from older sediments and rocks.

Ascorbic acid was highly efficient in extracting all Mn phosphates and vivianite-type minerals (>95%; Fig. 2), besides Mn oxides. The dissolution of the vivianite-type minerals slightly decreased with increasing Mn content, from 99% (Mn/Fe ratio: 0.1) to 96% for switzerite (the Mn-rich end-member), which could indicate that the mineral stability increases slightly when the Mn content in the minerals is high. The ascorbic acid solution did not dissolve Mn carbonates (<1%) but did dissolve some MnS (ca. 30%), as also observed by Hyacinthe and Van Cappellen (2004).

The 1 M HCl solution (Step 2) efficiently extracted Mn carbonate (99%) and Mn sulfide (70%; Fig. 2). A small amount of the crystalline Mn oxides, manganite (16%), bixbyite (9%) and hausmannite (11%), was extracted in 1 M HCl as well. This demonstrates that 1 M HCl mainly targets Mn carbonates and Mn sulfides and that these can be differentiated from the poorly ordered Mn oxides and Mn phosphates that are extracted in the first step of this method.

The CDB and ammonium oxalate solutions (Step 3 and 4) are widely used to extract crystalline Fe oxides, such as goethite, hematite and magnetite (Poulton and Canfield, 2005; Claff et al., 2010). We observed that the CDB and ammonium oxalate solutions extracted the remaining part of the crystalline Mn oxides (i.e. manganite, bixbyite and hausmannite; Fig. 2). However, because these Mn oxides were partly dissolved in the first two steps, poorly ordered and more crystalline Mn oxides cannot be fully separated via this procedure.

Concentrated HNO_3 (Step 5) is commonly used to extract pyrite and associated trace metals after the extraction of the other metal phases (Lord, 1982; Huerta-Diaz and Morse, 1992; Claff et al., 2010). Since no other Mn standards are extracted in the concentrated HNO_3 solution, this suggests that this step is indeed specific for Mn associated with pyrite. Part of the Mn in the smectites was extracted in all steps. However, the total extracted Mn concentrations were very low (<5 μmol g^{-1}; Fig. 2; Table A.1).

The kinetic experiments with ascorbic acid were performed on two minerals that were nearly completely dissolved in this step (i.e. poorly ordered Mn oxide (birnessite) and Mn bearing vivianite (Mn/Fe ratio: 0.1)) and one mineral that was partly dissolved (crystalline Mn oxide (manganite); Fig. 3). Dissolved Mn concentrations in the birnessite and Mn bearing vivianite experiment both reach a plateau after ca. 2.5 h, which indicates that the complete dissolution of these minerals occurs relatively fast (Fig. 3A and C). Concentrations of dissolved Fe and Mn versus time in the ascorbic acid extraction of Mn bearing vivianite were nearly identical. This suggests that the mineral dissolved homogeneously and that there is no preferential release of either Mn or Fe. Manganite dissolution does not reach a plateau in the experiment (Fig. 3B), which is in accordance with our observation that ca. 50% of manganite dissolved in the ascorbic acid solution during the 24 h extraction. In future experiments, the effect of shortening the extraction time of the ascorbic acid extraction might be assessed in more detail to improve the separation between poorly ordered Mn oxides, such as birnessite, and vivianite-type minerals and the crystalline Mn oxides, such as manganite.

3.2. Porewater Mn and Mn speciation in sediments

The sediments at the six study sites differ greatly in their porewater characteristics. The shape of the porewater profiles point towards production of dissolved Mn in the sediment at all locations (Burdige (2006); Fig. 4A). Porewater sulfide was present at all sites and either increases with depth (LL19, GoF5, Black Sea 6) or shows a subsurface maximum (GoM1, US5B, ET5.1). Concentrations are highest at the euxinic and seasonally hypoxic sites in the Baltic Sea (LL19, GoF5). These differences in sulfide availability are expected to impact both total Mn contents and the Mn speciation in the sediment (Burdige and Nealson, 1986).

Our total Mn analyses and the application of the sequential extraction procedure to the sediments from the six sites, ordered based on their bottom water redox conditions (euxinic to oxic; Table 3) confirm that there are large differences in sediment Mn contents and speciation (Figs. 4B and 5). Below, we discuss the Mn profiles for each site within the context of several key site characteristics, including what is known about the sediment forms of Mn based on previous studies (Table 4).

The porewaters at the euxinic site LL19 in the Baltic Sea are rich in both dissolved Mn and H_2S (maxima of ~70 and 250 μmol L^{-1}, respectively, Fig. 4A). The linear increase in dissolved Mn with depth points towards a Mn source below the sampled interval. Total sediment Mn contents (Fig. 4B) are mostly below 10 μmol g^{-1} except for the depths between 7 and 10 cm where they increase to ca. 100 μmol g^{-1} (Fig. 4B). At this site, only few Mn oxides are expected because of their rapid reduction with H_2S, either in the water column or sediment (Burdige, 1993). The subsurface maximum in total Mn at this site has previously been attributed to Mn carbonate precipitation linked to water column reoxygenation (Jilbert and Slomp, 2013; Lenz et al., 2015). The extraction data show that ascorbic acid extractable Mn contents are very low (Fig. 5A). A slight enrichment is observed near the sediment water interface, however, that may indicate that small amounts of poorly ordered Mn oxides can survive transport through a euxinic water column and be deposited at the sediment-water interface. At ca. 8 cm depth the majority of the Mn is extracted in the HCl step, which points towards the presence of Mn carbonate, in line with expectations. The CDB and ammonium oxalate extractable Mn is low and near constant with depth. The Mn extractable with HNO_3 is a small but detectable fraction, pointing towards incorporation of small amounts of Mn during the

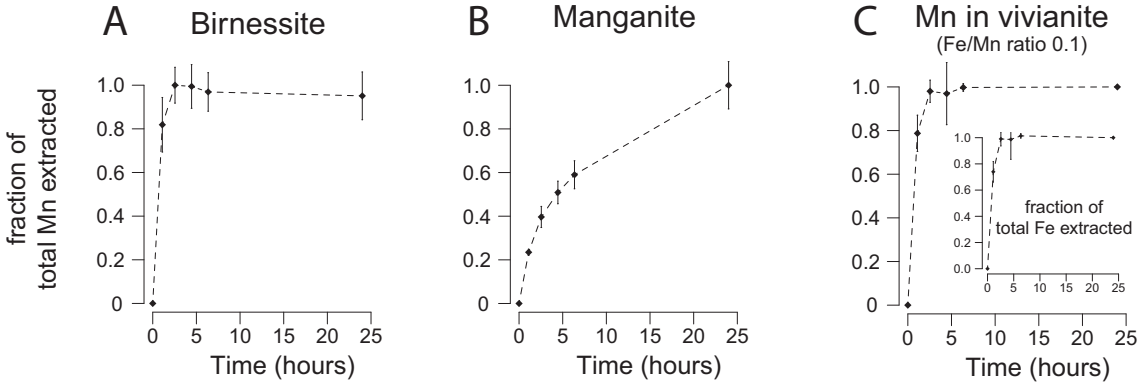

Fig. 3. Fraction of Mn (and Fe for the vivianite-type mineral) dissolved during the extraction of three Mn standards with ascorbic acid during 24 h (Step 1), A: birnessite, B: manganite and C: Mn bearing vivianite. Y axis represents the fraction of the Mn standard extracted in the 24 h ascorbic acid extraction. Data points represent the means of triplicate samples.

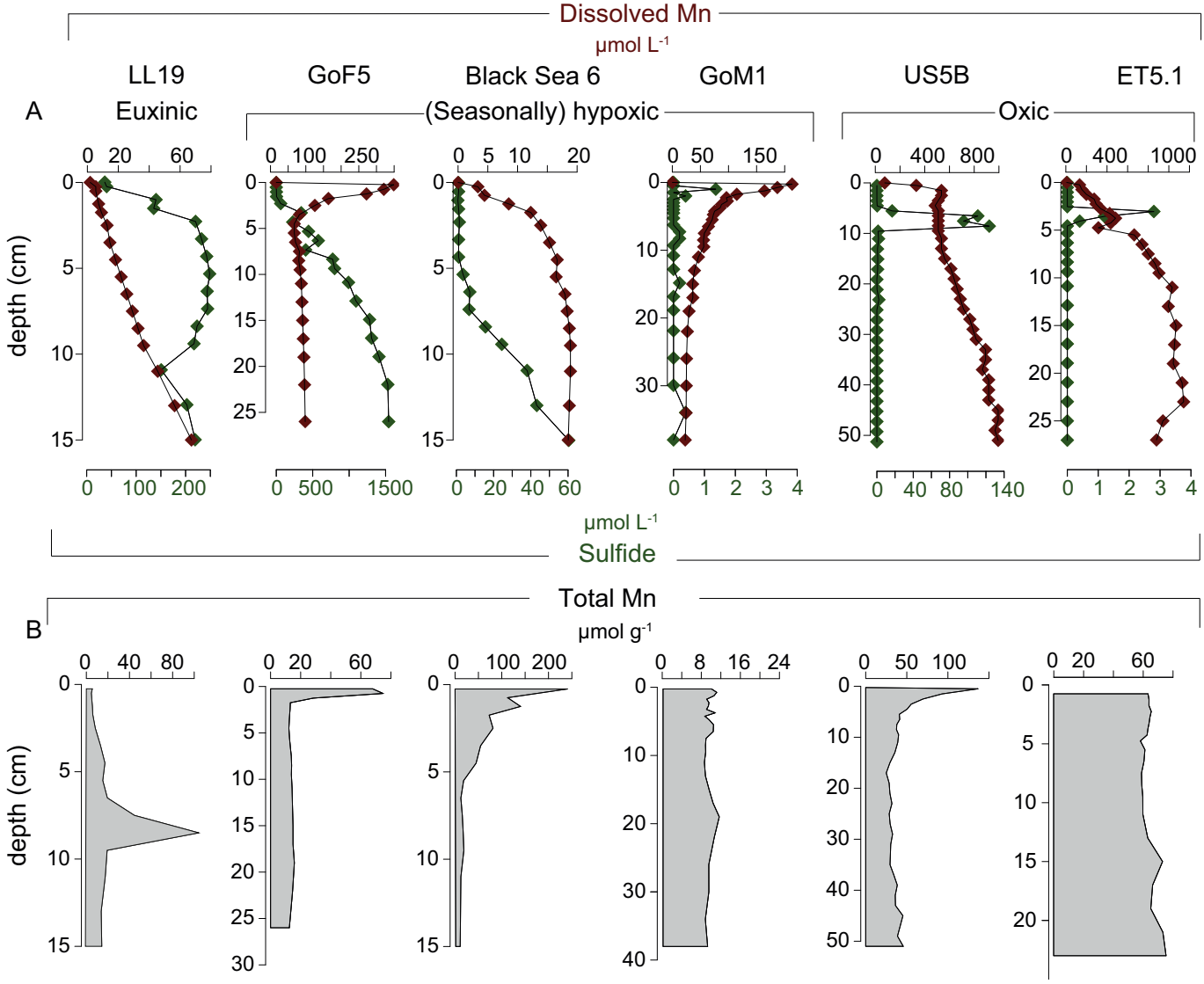

Fig. 4. Depth profiles for six sites investigated in this study. A: Porewater Mn and sulfide; B: solid phase Mn.

formation of pyrite. Such incorporation has been reported previously for sediments in the region, based on Mn-XANES (Lenz et al., 2014).

The porewaters at the (seasonally) hypoxic sites GoF5, Black Sea 6 and GoM1, located in the Baltic Sea, Black Sea and Gulf of Mexico, respectively, are all enriched in dissolved Mn and indicate mobilization of Mn from the solid phase in the upper 5 cm of the sediment. The observed maxima in porewater Mn at sites GoF5 and GoM1 are typically interpreted as indicators of Mn oxide dissolution near the sediment water interface and Mn carbonate formation at depth. At GoF5, a strong enrichment in ascorbic acid extractable Mn at the sediment-surface and the presence of HCl-extractable Mn at depth confirm this interpretation (Fig. 5). Ascorbic acid extractable Mn at site GoM1 is very low, which may be related to dilution because of the high sedimentation rate (ca. 2 cm yr^{-1}; Canfield (1988)), rapid dissolution of Mn oxides upon deposition and subsequent benthic release of dissolved Mn (Lenstra et al., in prep). The Black Sea site is located near the chemocline at the shelf edge of the deep euxinic basin.

Here, the Mn enrichment, in the nearly sulfide-free surface sediment, was expected to either consist of Mn oxides or Mn carbonates (Table 4). Our extraction results suggest that the Mn was extracted by HCl and hence consists mostly of Mn carbonates. At all three sites, the CDB and ammonium oxalate extractable Mn account for an appreciable and constant fraction of Mn, pointing towards burial of less reactive/nonreactive Mn forms in the sediment. At sites GoF5 and GoM1, Mn is extracted in the HNO_3 step when pyrite concentrations are above 40 µmol g^{-1} (Fig. A.2). This suggests that when pyrite contents and dissolved manganese concentrations are both sufficiently high, Mn can be incorporated in the pyrite structure.

The porewaters at the sites with oxic bottom waters, US5B and ET5.1, located in the Bothnian Sea and Chesapeake Bay, are highly enriched in dissolved Mn (>1000 µmol L^{-1}) with concentrations increasing with sediment depth. The subsurface maximum in dissolved H_2S at both sites is linked to methane oxidation with sulfate (Egger et al., 2015; Kubeneck et al., 2021). At both sites, sink-switching of Mn from Mn oxides to Mn bearing vivianite-type minerals has been proposed (Egger et al., 2015; Kubeneck et al., 2021). At both sites, Mn extractable with ascorbic acid was elevated near the sediment-water interface but also at depth (Fig. 5C). Because both Mn oxides and Mn phosphates are extracted in the ascorbic acid step, we cannot differentiate between Mn oxides and Mn in vivianite-type minerals. The slight increase in HCl-extractable Mn with depth suggests the formation of Mn carbonates. CDB and ammonium oxalate extractable Mn contribute an appreciable and constant fraction. Manganese associated with pyrite is below the detection limit at these sites, in line with the low pyrite content

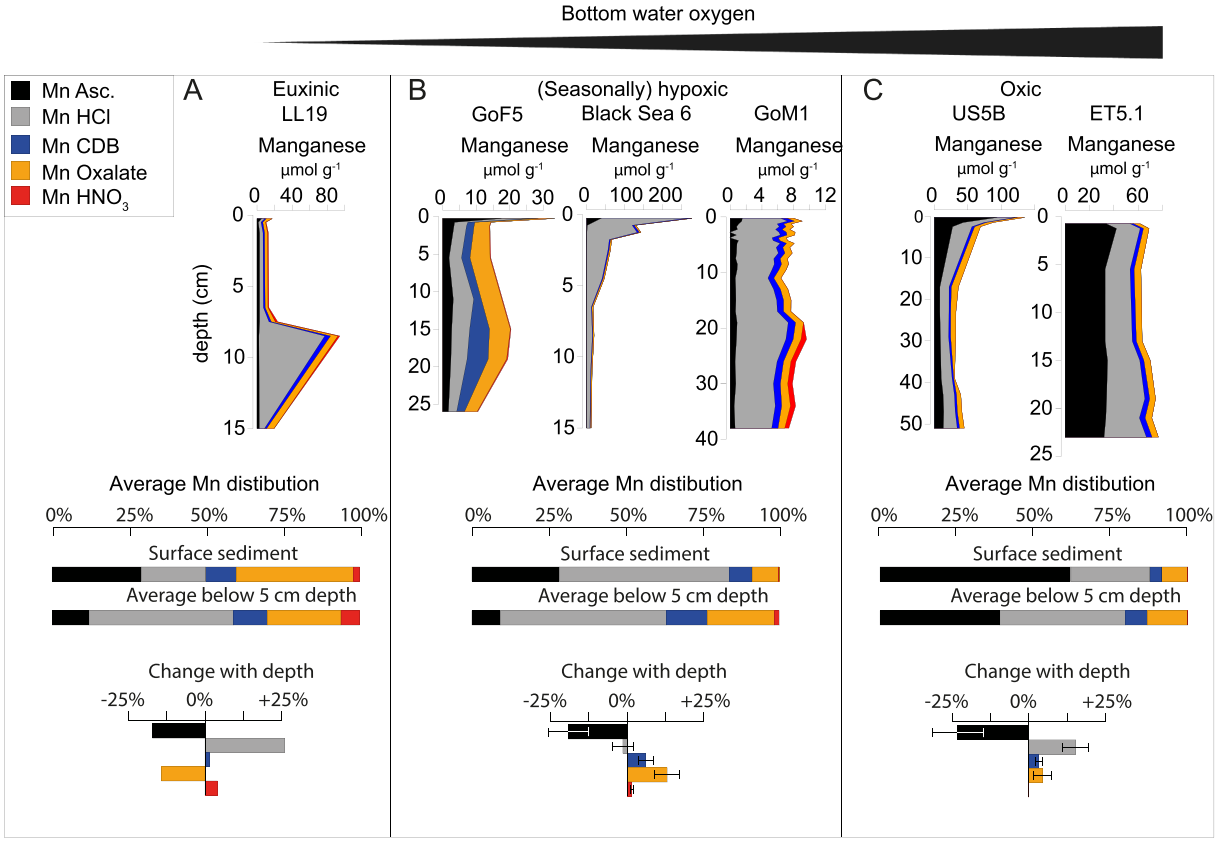

Fig. 5. Depth profiles of different forms of Mn at six sites as determined with the sequential extraction procedure, average distribution of Mn extracted in surface sediment and below 5 cm for non-sulfidic sites and change with depth of the different extracted Mn phases for A: euxinic site LL19; B: (seasonally) hypoxic sites GoF5, Black Sea 6 and GoM1; C: oxic sites US5B and ET5.1. The peak of Mn at ca. 8 cm depth at site LL19 is related to an inflow event of oxygen-rich water resulting in the deposition of high concentrations of Mn. The relatively low sample resolution at LL19 is the cause of the broad Mn peak in panel A (see Fig. 4 and the supplementary data).

Table 4
Expected main Mn forms in the surface sediment (0–2 cm) and deeper sediment (below 5 cm) based on previous studies.

Site	Surface sediment	Deeper sediment	Method	Source
LL19	Small amount of Mn oxides	Mn carbonates	µXRF[a]	Lenz et al. (2015)
GoF5	Mn oxides and/or Mn phosphates	Non-reactive Mn	Mn-XANES & µXRF[b]	Hermans et al. (2021)
Black Sea 6	Mn oxides and/or Mn carbonates	Non-reactive Mn	Mn-XANES &Mn-EXAFS	Lenstra et al. (2021)
GoM1	Mn oxides	Mn carbonates	–	(Lenstra et al., in prep.)
US5B	Mn oxides	Mn oxides/Mn phosphates	SEM-EDS, µXRF[a, b] Mn-XANES	Egger et al. (2015)
ET5.1	Mn oxides	Mn oxides/Mn phosphates	SEM-EDS & µXRF[a]	Kubeneck et al. (2021)

[a] Desktop µ X-Ray Fluorescence (µXRF).
[b] Synchrotron-based focused-beam µXRF.
SEM-EDS: Scanning Electron Microscopy – Energy Dispersive X-ray Spectroscopy.
Mn-EXAFS: Extended X-ray Absorption Fine Structure.
Mn-XANES: X-ray Absorption Near-Edge Structure.

(<45 µmol g^{-1}; Fig. A.2).

3.3. Implications and conclusions

In this study we applied an existing sequential extraction procedure for Fe on a range of Mn standards consisting of Mn oxides, Mn phosphates, Mn carbonate, Mn sulfide and Mn in clays (Table 1 and A.1). The ascorbic acid solution (Step 1) was efficient in extracting poorly ordered Mn oxides, such as birnessite and pyrolusite, and Mn phosphates. Additionally, ascorbic acid partly extracted crystalline Mn oxides, such as manganite and hausmannite. The 1 M HCl (Step 2) was highly efficient in extracting Mn carbonate and Mn sulfide. Since Mn sulfides are only observed in highly sulfidic systems (e.g. Suess (1979), Lepland and Stevens (1998)), we expect that 1 M HCl predominantly extracts Mn carbonates in marine systems. To detect the possible presence of Mn sulfides other techniques such as XRD, SEM-EDS or XANES/EXAFS, are required. The CDB and ammonium oxalate solutions (Step 3 and 4), extracted the remainder of the crystalline Mn oxides. These crystalline Mn oxides were partially extracted in the previous steps, therefore step 3 and 4 are not specific for Mn oxides with a high crystallinity. The concentrated HNO_3 solution (Step 5) extracted a negligible amount of the Mn standards (Fig. 2; Table A.1) but has been shown to be highly efficient in extracting pyrite in a sequential extraction procedure (Lord, 1982; Huerta-Diaz and Morse, 1992; Claff et al., 2010). Therefore this step is likely specific for Mn incorporated in pyrite.

Application of the extraction procedure to a range of coastal sediments shows how the results complement those of total Mn and X-ray analyses in allowing a quantification of the various sediment Mn forms for a large number of samples. Our extraction results also highlight a

number of key aspects of Mn cycling in coastal systems. These are discussed one by one below.

In euxinic coastal marine basins, Mn oxides (or mixed Fe-Mn-P phases) formed in the redoxcline, are expected to be reductively dissolved by H_2S before they reach the surface sediment (e.g. (Dellwig et al., 2010; Dijkstra et al., 2018b). Any Mn detected in such sediments is thought to be associated with either pyrite or clays (Lyons and Severmann, 2006; Lenstra et al., 2020). We find, however, that at the euxinic site in the Baltic Sea, ascorbic acid extractable Mn accounts for ca. 30% of the total Mn pool in the surface sediment, with concentrations quickly decreasing with sediment depth (Fig. 5A). This suggests that some Mn oxides and/or mixed Fe-Mn-P phases survive transport through the euxinic water column and are deposited at the sediment water interface. This may be due to the shallow water euxinic column at our Baltic Sea study site (80 m versus 2000 m in the Black Sea), possibly augmented by rapid sinking and shuttling of Mn-rich particles upon their association with other inorganic or organic particles (e.g. Martin and Knauer (1980)).

At sites with (seasonally) hypoxic bottom waters, the Mn speciation of surface sediments will depend on a range of factors including bottom water oxygen concentrations, the input of Mn oxides from the water column, and the presence of reductants in the sediment, such as organic matter and porewater sulfide (Burdige, 1993). Given that our study sites in the Baltic Sea, Black Sea and Gulf of Mexico show large differences in such characteristics (Table 3; Fig. 4), it is not surprising that their Mn speciation in the surface sediment also differs. At site GoF5, rapid cycling of Mn between the surface sediment and the redoxcline in the water column likely explains the enrichment in Mn oxides near the sediment surface in these otherwise highly reducing sediments (Figs. 4 and 5) as discussed in detail by Hermans et al. (2021). At the Black Sea site near the redoxcline, in contrast, most Mn in the surface sediment is present as Mn carbonate, pointing towards conversion of Mn oxides to Mn carbonates in these sulfide-poor shelf sediments. Based on the shape of the total sediment Mn profile, this Mn could have been wrongly assigned to Mn oxides if no Mn speciation data were available. At site GoM1, very little Mn oxide is present in the surface sediment, likely due to rapid mobilization in the sediment and diffusive loss of dissolved Mn to the water column (Figs. 4 and 5), possibly followed by offshore transport of the Mn (Bianchi et al., 1997; Owings et al., 2021).

At our sites with oxic bottom waters, both the surface and deeper sediments contain quite some ascorbic acid extractable Mn. While in the surface sediment this Mn fraction likely consists of Mn oxides, at depth Mn-rich vivianite plays an additional role as deduced from a range of microscopic and X-ray analyses of the sediment at these sites (Egger et al., 2015; Kubeneck et al., 2021). Vivianite is frequently formed below the sulfate-methane-transition zone in marine sediments (Marz et al., 2008; Egger et al., 2015; Lenstra et al., 2018), and while its role as a sink for P is well-recognized, its contribution to Mn burial deserves further study. Further work is also needed to establish what types of Mn oxides may be buried in coastal sediments and their potential role in, for example, anaerobic methane oxidation (e.g. Beal et al. (2009)).

At all sites, the relative contribution of 1 M HCl extractable Mn to total Mn increased with sediment depth (Fig. 5). At the euxinic site, the sharp increase in Mn between 7 and 10 cm (Figs. 4 and 5) can be linked to an inflow of oxygenated North Sea water into the Gotland basin, subsequent deposition of newly formed Mn oxides at the sediment surface and their rapid conversion to Mn carbonate (Lenz et al., 2015). At many of the other sites, some sink-switching of Mn oxides to Mn carbonates likely also occurs, although this is much less pronounced. Importantly, our study sites are all characterized by either no macrofauna or low numbers thereof, and hence, low rates of sediment mixing through bioturbation (Hermans et al., 2019; Lenstra et al., 2019; Egger et al., 2015; Kubeneck et al., 2021). The presence of Mn carbonate near the sediment water interface therefore suggests rapid formation of this mineral near the sediment water interface and/or input from the water column. We note that suspended matter in the Baltic Sea and Black Sea contains 1 M HCl extractable Mn (Lenstra et al., 2020, 2021), supporting the latter suggestion.

At all sites, CDB and ammonium oxalate extractable Mn accounted for a constant background concentration of Mn. This suggests that the associated Mn phases are non-reactive, and most likely involve recalcitrant Mn oxides or Mn in clays. Additionally, part of the Mn released in the ammonium oxalate step might be Mn that was readsorbed onto crystalline Fe oxides during previous extraction steps (Koschinsky et al., 2001). Finally, we show that HNO_3 extractable Mn is a small but detectable fraction that increases slightly with depth at sites where pyrite concentrations are relatively high, in line with incorporation of Mn in pyrite.

With the use of this new sequential extraction procedure for particulate Mn, it is possible to determine key operationally defined Mn forms in sediments simultaneously with those of Fe. This has large benefits for the study of Mn and Fe dynamics in marine sediments, as illustrated here for Mn for six coastal sites with strongly contrasting bottom water redox conditions. We envisage that this procedure will also be of benefit when studying ancient marine sediments, by allowing a quick separation of Mn oxides and Mn carbonates. Sediments in the eastern Mediterranean Sea, for example, are characterized by an enrichment in total Mn at or near the top of the most recent sapropel. This enrichment usually consists of Mn oxides but, in some cases, the Mn oxides may convert to Mn carbonate. This was, for example, demonstrated for a highly Mn-enriched sediment in the Aegean Sea using X-ray diffraction (Mercone et al., 2001). Our procedure should allow such cases to be identified, also when sediment Mn contents are lower. Similarly, the extraction procedure could be used to assess the composition of Mn-rich layers in ancient Arctic Ocean sediments where, besides diagenetically formed Mn carbonates, buried Mn oxide layers are observed (e.g. Lowemark et al., (2014)). We note, however, that the current technique is not calibrated for the quantification of the widely used highly reactive Fe parameter in ancient sediments (Raiswell et al., 2018; Alcott et al., 2020). The value of the extraction procedure for the analysis of Fe and Mn in suspended matter was illustrated previously (Lenstra et al., 2020, 2021).

Data availability

All data is available in the supplementary material of this publication.

Declaration of Competing Interest

The authors declare no conflict of interest.

Acknowledgements

We thank C. Mulder, H. de Waard, N. van Helmond and A. van Leeuwen-Tolboom for analytical assistance. This research was funded by the Netherlands Organisation for Scientific Research (NWO-Vici grant 865.13.005), Netherlands Earth System Science Centre (NESSC Gravitation grant 024.002.001) and ERC (ERC synergy MARIX grant 854088).

Appendix A. Supplementary data

Supplementary data to this article can be found online at https://doi.org/10.1016/j.chemgeo.2021.120538.

References

Alcott, L.J., et al., 2020. Development of iron speciation reference materials for palaeoredox analysis. Geostand. Geoanal. Res. 44, 581–591.
Anschutz, P., Dedieu, K., Desmazes, F., Chaillou, G., 2005. Speciation, oxidation state, and reactivity of particulate manganese in marine sediments. Chem. Geol. 218, 265–279.

Beal, E.J., House, C.H., Orphan, V.J., 2009. Manganese- and iron-dependent marine methane oxidation. Science 325, 184–187.
Bianchi, T.S., Lambert, C.D., Santschi, P.H., Guo, L., 1997. Sources and transport of land-derived particulate and dissolved organic matter in the Gulf of Mexico (Texas shelf/slope): the use of ligninphenols and loliolides as biomarkers. Org. Geochem. 27, 65–78.
Breitburg, D., et al., 2018. Declining oxygen in the global ocean and coastal waters. Science 359, eaam7240.
Brumsack, H.J., 2006. The trace metal content of recent organic carbon-rich sediments: implications for cretaceous black shale formation. Palaeogeogr. Palaeoclimatol. Palaeoecol. 232, 344–361.
Burdige, D.J., 1993. The biogeochemistry of manganese and iron reduction in marine sediments. Earth Sci. Rev. 35, 249–284.
Burdige, D.J., 2006. Geochemistry of Marine Sediments. Princeton University Press.
Burdige, D.J., Nealson, K.H., 1986. Chemical and microbiological studies of sulfide mediated manganese reduction. Geomicrobiol. J. 4, 361–387.
Calvert, S., Pedersen, T., 1993. Geochemistry of recent oxic and anoxic marine sediments: implications for the geological record. Mar. Geol. 113, 67–88.
Canfield, D.E., 1988. Reactive iron in marine sediments. Geochim. Cosmochim. Acta 53, 619–632.
Canfield, D.E., et al., 1993. Pathways of organic carbon oxidation in three continental margin sediments. Mar. Geol. 133, 27–40.
Claff, S.R., Sullivan, L.A., Burton, E.D., Bush, R.T., 2010. A sequential extraction procedure for acid sulfate soils: partitioning of iron. Geoderma 155, 224–230.
Dellwig, O., Bosselmann, K., K“olsch, S., Hentscher, M., Hinrichs, J., B” ottcher, M.E., Reuter, R., Brumsack, H.-J., 2007. Sources and fate of manganese in a tidal basin of the German Wadden Sea. J. Sea Res. 57, 1–18.
Dellwig, O., Leipe, T., M“arz, C., Glockzin, M., Pollehne, F., Schnetger, B., Yakushev, E.V., B”ottcher, M.E., Brumsack, H.J., 2010. A new particulate Mn-Fe-P-shuttle at the redoxcline of anoxic basins. Geochim. Cosmochim. Acta 74, 7100–7115.
Dijkstra, N., Hagens, M., Egger, M., Slomp, C.P., 2018a. Post-depositional formation of vivianite-type minerals alters sediment phosphorus records. Biogeosciences 15, 861–883.
Dijkstra, N., Kraal, P., Séguret, M.J., Flores, M.R., Gonzalez, S., Rijkenberg, M.J., Slomp, C.P., 2018b. Phosphorus dynamics in and below the redoxcline in the Black Sea and implications for phosphorus burial. Geochim. Cosmochim. Acta 222, 685–703.
Egger, M., Jilbert, T., Behrends, T., Rivard, C., Slomp, C.P., 2015. Vivianite is a major sink for phosphorus in methanogenic coastal surface sediments. Geochim. Cosmochim. Acta 169, 217–235.
Eitel, E.M., Zhao, S., Tang, Y., Taillefert, M., 2018. Effect of manganese oxide aging and structure transformation on the kinetics of thiol oxidation. Environ. Sci. Technol. 52, 13202–13211.
Goldberg, E.D., 1954. Marine Geochemistry 1. Chemical Scavengers of the Sea. J. Geol. 62, 249–265.
Hem, J.D., Lind, C.J., 1983. Nonequilibrium models for predicting forms of precipitated manganese oxides. Geochim. Cosmochim. Acta 47, 2037–2046.
Hermans, M., Lenstra, W.K., Hidalgo-Martinez, S., van Helmond, N.A.G.M., Witbaard, R., Meysman, F.J., Gonzalez, S., Slomp, C.P., 2019. Abundance and biogeochemical impact of cable bacteria in baltic sea sediments. Environ. Sci. Technol. 53, 7494–7503.
Hermans, M., Astudillo Pascual, M., Behrends, T., Lenstra, W.K., Conley, D.J., Slomp, C. P., 2021. Coupled dynamics of iron, manganese, and phosphorus in brackish coastal sediments populated by cable bacteria. Limnol. Oceanogr. 1–21.
Huerta-Diaz, M.A., Morse, J.W., 1990. A quantitative method for determination of trace metal concentrations in sedimentary pyrite. Mar. Chem. 29, 119–144.
Huerta-Diaz, M.A., Morse, J.W., 1992. Pyritization of trace metals in anoxic marine sediments. Geochim. Cosmochim. Acta 56, 2681–2702.
Hyacinthe, C., Van Cappellen, P., 2004. An authigenic iron phosphate phase in estuarine sediments: composition, formation and chemical reactivity. Mar. Chem. 91, 227–251.
Hyacinthe, C., Anschutz, P., Carbonel, P., Jouanneau, J.-M., Jorissen, F.J., 2001. Early diagenetic processes in the muddy sediments of the Bay of Biscay. Mar. Geol. 177, 111–128.
Jilbert, T., Slomp, C.P., 2013. Iron and manganese shuttles control the formation of authigenic phosphorus minerals in the euxinic basins of the Baltic Sea. Geochim. Cosmochim. Acta 107, 155–169.
Johnson, J.E., Webb, S.M., Ma, C., Fischer, W.W., 2016. Manganese mineralogy and diagenesis in the sedimentary rock record. Geochim. Cosmochim. Acta 173, 210–231.
Kester, D.R., Duedall, I.W., Connors, D.N., Pytkowicz, R.M., 1967. Preparation of artificial seawater. Limnol. Oceanogr. 12, 176–179.
Koschinsky, A., Hein, J.R., 2003. Uptake of elements from seawater by ferromanganese crusts: solid-phase associations and seawater speciation. Mar. Geol. 198, 331–351.
Koschinsky, A., Fritsche, U., Winkler, A., 2001. Sequential leaching of Peru Basin surface sediment for the assessment of aged and fresh heavy metal associations and mobility. Deep-Sea Res. Part II: Top. Stud. Oceanogr. 48, 3683–3699.
Kubeneck, L.J., Lenstra, W.K., Malkin, S.Y., Conley, D.J., Slomp, C.P., 2021. Phosphorus burial in vivianite-type minerals in methane-rich coastal sediments. Mar. Chem. 103948.
Lam, P.J., Twining, B.S., Jeandel, C., Roychoudhury, A., Resing, J.A., Santschi, P.H., Anderson, R.F., 2015. Methods for analyzing the concentration and speciation of major and trace elements in marine particles. Prog. Oceanogr. 133, 32–42.
Learman, D.R., Wankel, S.D., Webb, S.M., Martinez, N., Madden, A.S., Hansel, C.M., 2011. Coupled biotic-abiotic Mn(II) oxidation pathway mediates the formation and structural evolution of biogenic Mn oxides. Geochim. Cosmochim. Acta 75, 6048–6063.
Lee, J.-M., et al., 2021. Changing chemistry of particulate manganese in the near-and far-field hydrothermal plumes from 15° S East Pacific rise and its influence on metal scavenging. Geochim. Cosmochim. Acta 300, 95–118.
Lenstra, W.K., Egger, M., van Helmond, N.A.G.M., Kritzberg, E., Conley, D.J., Slomp, C. P., 2018. Large variations in iron input to an oligotrophic Baltic Sea estuary: impact on sedimentary phosphorus burial. Biogeosciences.
Lenstra, W.K., Séguret, M.J.M., Behrends, T., Groeneveld, R.K., Hermans, M., Witbaard, R., Slomp, C.P., 2020. Controls on the shuttling of manganese over the northwestern Black Sea shelf and its fate in the euxinic deep basin. Geochim. Cosmochim. Acta 273, 177–204.
Lenstra, W.K., Hermans, M., Séguret, M.J.M., Witbaard, R., Severmann, S., Behrends, T., Slomp, C.P., 2021. Coastal hypoxia and eutrophication as key controls on benthic release and water column dynamics of iron and manganese. Limnol. Oceanogr. 66, 807–826.
Lenstra, W.K., et al., 2019. The shelf-to-basin iron shuttle in the Black Sea revisited. Chem. Geol. 511, 314–341.
Lenstra, W. K., N. A. G. M. van Helmond, O. Zygadlowska, R. Witbaard, and C. P. Slomp, Sediments as a source of iron, manganese, cobalt and nickel to continental shelf waters (Louisiana, Gulf of Mexico), in prep.
Lenz, C., Behrends, T., Jilbert, T., Silveira, M., Slomp, C.P., 2014. Redox-dependent changes in manganese speciation in Baltic Sea sediments from the holocene thermal maximum: an EXAFS, XANES and LA-ICP-MS study. Chem. Geol. 370, 49–57.
Lenz, C., Jilbert, T., Conley, D.J., Slomp, C.P., 2015. Hypoxia-driven variations in iron and manganese shuttling in the Baltic Sea over the past 8 kyr. Geochem. Geophys. Geosyst. 16, 3754–3766.
Lepland, A., Stevens, R.L., 1998. Manganese authigenesis in the Landsort Deep, Baltic Sea. Mar. Geol. 151, 1–25.
Lord III, C.J., 1982. A selective and precise method for pyrite determination in sedimentary materials: research-method paper. J. Sediment. Res. 52.
Lowemark, L., M”arz, C., O'Regan, M., Gyllencreutz, R., 2014. Arctic Ocean Mn-stratigraphy: genesis, synthesis and inter-basin correlation. Q. Sci. Rev. 92, 97–111.
Luther III, G.W., Sundby, B., Lewis, B.L., Brendel, P.J., Silverberg, N., 1997. Interactions of manganese with the nitrogen cycle: alternative pathways to dinitrogen. Geochim. Cosmochim. Acta 61, 4043–4052.
Lyons, T.W., Severmann, S., 2006. A critical look at iron paleoredox proxies: new insights from modern euxinic marine basins. Geochim. Cosmochim. Acta 70, 5698–5722.
Madison, A.S., Tebo, B.M., Mucci, A., Sundby, B., Luther, G.W., 2013. Abundant porewater Mn(III) is a major component of the sedimentary redox system. Science 341.
Martin, J.H., Knauer, G.A., 1980. Manganese cycling in northeast Pacific waters. Earth Planet. Sci. Lett. 51, 266–274.
Marz, C., Hoffmann, J., Bleil, U., de Lange, G.J., Kasten, S., 2008. Diagenetic changes of magnetic and geochemical signals by anaerobic methane oxidation in sediments of the Zambezi deep-sea fan (SW Indian Ocean). Mar. Geol. 255, 118–130.
Mercone, D., Thomson, J., Abu-Zied, R.H., Croudace, I.W., Rohling, E.J., 2001. High-resolution geochemical and micropalaeontological profiling of the most recent Eastern Mediterranean sapropel. Mar. Geol. 177, 25–44.
Middelburg, J.J., De Lange, G.J., van Der Weijden, C.H., 1987. Manganese solubility control in marine pore waters. Geochim. Cosmochim. Acta 51, 759–763.
Millero, F.J., 1974. Seawater as a multicomponent electrolyte solution. In: The Sea, Volume 5, Marine Chemistry, pp. 3–80.
Moore, C.M., et al., 2013. Processes and patterns of oceanic nutrient limitation. Nat. Geosci. 6, 701–710.
Mouret, A., et al., 2009. Benthic geochemistry of manganese in the Bay of Biscay, and sediment mass accumulation rate. Geo-Mar. Lett. 29, 133–149.
Mucci, A., 1988. Manganese uptake during calcite precipitation from seawater: conditions leading to the formation of a pseudokutnahorite. Geochim. Cosmochim. Acta 52, 1859–1868.
Nakano, S., 1992. Manganoan vivianite in the bottom sediments of Lake Biwa, Japan. Mineral. J. 16, 96–107.
Neumann, T., Heiser, U., Leosson, M.A., Kersten, M., 2002. Early diagenetic processes during Mn-carbonate formation: evidence from the isotopic composition of authigenic Ca-rhodochrosites of the Baltic Sea. Geochim. Cosmochim. Acta 66, 867–879.
Ostrander, C.M., Nielsen, S.G., Owens, J.D., Kendall, B., Gordon, G.W., Romaniello, S.J., Anbar, A.D., 2019. Fully oxygenated water columns over continental shelves before the Great Oxidation Event. Nat. Geosci. 12, 186–191.
Owings, S.M., et al., 2021. Differential manganese and iron recycling and transport in continental margin sediments of the Northern Gulf of Mexico. Mar. Chem. 229, 103908.
Postma, D., 1985. Concentration of Mn and separation from Fe in sediments-I. Kinetics and stoichiometry of the reaction between birnessite and dissolved Fe(II) at 10 degrees C. Geochim. Cosmochim. Acta 49, 1023–1033.
Poulton, S.W., Canfield, D.E., 2005. Development of a sequential extraction procedure for iron: implications for iron partitioning in continentally derived particulates. Chem. Geol. 214, 209–221.
Raiswell, R., Vu, H.P., Brinza, L., Benning, L.G., 2010. The determination of labile Fe in ferrihydrite by ascorbic acid extraction: methodology, dissolution kinetics and loss of solubility with age and de-watering. Chem. Geol. 278, 70–79.
Raiswell, R., Hardisty, D.S., Lyons, T.W., Canfield, D.E., Owens, J.D., Planavsky, N.J., Poulton, S.W., Reinhard, C.T., 2018. The iron paleoredox proxies: a guide to the pitfalls, problems and proper practice. Am. J. Sci.

Raven, J.A., 1990. Predictions of Mn and Fe use efficiencies of phototrophic growth as a function of light availability for growth and of C assimilation pathway. New Phytol. 116, 1–18.
Rouzies, D., Millet, J.M., 1993. M”ossbauer study of synthetic oxidized vivianite at room temperature. Hyperfine Interact. 77, 19–28.
Suess, E., 1979. Mineral phases formed in anoxic sediments by microbial decomposition of organic matter. Geochim. Cosmochim. Acta 43, 399–352.
Sulu-Gambari, F., Roepert, A., Jilbert, T., Hagens, M., Meysman, F.J.R., Slomp, C.P., 2017. Molybdenum dynamics in sediments of a seasonally-hypoxic coastal marine basin. Chem. Geol. 466, 627–640.
Sundby, B., Silverberg, N., 1985. Manganese fluxes in the benthic boundary layer. Limnol. Oceanogr. 30, 372–381.
Tessier, A., Campbell, P.G., Bisson, M., 1979. Sequential Extraction Procedure for the Speciation of Particulate Trace Metals. Anal. Chem.